Physica B: Condensed Matter 531 (2018) 216–222

Contents lists available at ScienceDirect

Physica B: Condensed Matter

journal homepage: www.elsevier.com/locate/physb

Electronic, thermodynamics and mechanical properties of LaB_6 from first-principles

V.I. Ivashchenko [a,*], P.E.A. Turchi [b], V.I. Shevchenko [a], N.R. Medukh [a], Jerzy Leszczynski [c], Leonid Gorb [c,d]

[a] Institute of Problems of Material Science, NAS of Ukraine, Krzhyzhanovsky str. 3, 03680 Kyiv, Ukraine
[b] Lawrence Livermore National Laboratory, L-352, P.O. Box 808, Livermore, CA 94551, USA
[c] Department of Chemistry and Biochemistry, Interdisciplinary Center for Nanotoxicity, Jackson State University, Jackson, MS 39217, USA
[d] Badger Technical Services, LLC, Vicksburg, MS 39180, USA

ARTICLE INFO

Keywords:
Crystalline and amorphous LaB_6
First-principles calculations
Electronic structure
Elastic moduli
Thermodynamic and mechanical properties

ABSTRACT

Up to date, the electronic structure properties of amorphous lanthanum hexaboride, a-LaB_6, were not yet investigated, and the thermodynamic and mechanical properties of crystalline lanthanum hexaboride (c-LaB_6) were studied incompletely. The goal of this work was to fill these gaps in the study of lanthanum hexaborides. The electronic and phonon structures, thermodynamic and mechanical properties of both crystalline and amorphous lanthanum hexaborides (c-LaB_6, a-LaB_6, respectively) were investigated within the density functional theory. An amorphyzation of c-LaB_6 gives rise to the metal – semiconductor transition. The thermal conductivity decreases on going from c-LaB_6 to a-LaB_6. The elastic moduli, hardness, ideal tensile and shear strengths of a-LaB_6 are significantly lower compared to those of the crystalline counterpart, despite the formation of the icosahedron-like boron network in the amorphous phase. For c-LaB_6, the stable boron octahedrons are preserved after the failure under tensile and shear strains. The peculiarity in the temperature dependence of heat capacity, $C_p(T)$, at 50 K is explained by the availability of a sharp peak at 100 cm^{-1} in the phonon density of states of c-LaB_6. An analysis of the Fermi surface indicates that this peak is not related to the shape of the Fermi surface, and is caused by the vibration of lanthanum atoms. In the phonon spectrum of a-LaB_6, the peak at 100 cm^{-1} is significantly broader than in the spectrum of c-LaB_6, for which reason the anomaly in the $C_p(T)$ dependence of a-LaB_6 does not appear. The calculated characteristics are in good agreement with the available experimental data.

1. Introduction

Lanthanum hexaboride, LaB_6, crystallizing with a simple cubic structure (space group Pm3m, No. 221) is very promising material for industrial applications due to its high thermal stability, melting temperature, hardness and chemical stability [1–3]. LaB_6 is widely used as an electron emitter with a low work function (~2.4–2.6 eV) [3] and as a standard reference material for the calibration of the line position of powder diffraction instruments [1–4].

Up to date, bulk LaB_6 was comprehensively explored, whereas the films based on this material were studied to a lesser extent [5]. LaB_6 films have been prepared by using different deposition techniques. The crystalline (c), polycrystalline (pc) and amorphous (a) films were prepared depending on a procedures used and deposition conditions [5–7]. In contrast to the c- and pc- LaB_6 films, the amorphous films are studied incompletely. In fact, their investigation is in an infant stage. In particular, Nabauer [1] reported the results of the investigations of the a-LaB_6 films deposited on the GaAs substrates with the (100) orientation. The films were deposited by magnetron sputtering an amorphous LaB_6 target. It was found that the structural and electrical properties of the deposited films strongly depended on the parameters of the deposition process. Choi et al. [2] used the local microheating of amorphous LaB_6 films to achieve a micrometer-sized thermionic electron emission source with the maximum current density of 1.2 A/cm^2.

Theoretical investigations of c-LaB_6 were concentrated on the analysis of its electronic structure and bonding configuration. A comprehensive review of the theoretical studies up to 2005 year was done in Ref. [8]. Below we note only the more recent works. The optoelectronic properties of c-LaB_6 were calculated using first-principles molecular dynamics simulations [9]: the dielectric functions, refractive index,

* Corresponding author.
E-mail address: ivashchenko@icnanotox.org (V.I. Ivashchenko).

https://doi.org/10.1016/j.physb.2017.12.044
Received 26 October 2017; Received in revised form 13 December 2017; Accepted 14 December 2017
Available online 16 December 2017

reflection spectra, optical conductivity, absorption spectra, and energy loss function were analyzed. The optical properties of Yb-doped LaB_6 were investigated by first-principles calculations within the framework of the density functional theory (DFT) [10]. The electronic structure, phonons and optical properties of c-LaB_6 as functions of pressure were studied by using first-principles calculations [11]. First-principles calculations [12–15] were carried out to investigate the elastic constants of rare-earth hexaborides. The electronic structures, mechanical and thermodynamic properties of alkaline-earth hexaborides were calculated from first principles using DFT combined with the quasi-harmonic approximation [16]. The quality of the experimental charge densities for LaB_6 and BaB_6 was evaluated by comparison with theoretical charge densities [17].

This brief report points to that, despite the substantial amount of experimental and theoretical information accumulated on LaB_6, some important questions have not been yet addressed. Among them it is worth mentioning the following: 1) there are no theoretical investigations of the thermodynamics properties of c-LaB_6 and its mechanical properties were studied incompletely; 2) up today, the electronic, thermodynamics and mechanical properties of a-LaB_6 were not yet investigated. Therefore, we focused our attention on these questions. In this work we aim at filling these gaps in studying the properties of both c- and a-LaB_6 in the framework of a first-principles approach.

2. Computational details

First-principles calculations within the density functional theory (DFT) were carried out for the 7-atom cubic cell (stoichiometric c-LaB_6), the 6-atom cubic cell (substoichiometric c-LaB_5) and the 56-atom supercell (a-LaB_6) using the Quantum-ESPRESSO code [18]. The valence states for La and B were 5s, 5p, 5d, 6s, 6p, 4f and 2s, 2p, respectively. We consider the La 4f states as the valence ones, since they were found to contribute to the density of states near the Fermi level [19,20]. The calculations were performed using periodic boundary conditions and the generalized gradient approximation (GGA) of Perdew, Burke and Ernzerhof (PBE) [21] for the exchange-correlation energy and potential. Vanderbilt ultra-soft pseudo-potentials were used to describe the electron-ion interaction [22]. The criterion of convergence for the total energy was 10^{-6} Ry/formula unit (*i.e.*, $1.36{\cdot}10^{-5}$ eV/formula unit). In order to speed up the convergence, each eigenvalue was convoluted by a Gaussian with a width $\sigma = 0.02$ Ry (0.272 eV). The integration in the Brillouin zone (BZ) was done on a set of special k-points determined according to the Monkhorst–Pack scheme using a non-shifted meshes (12 12 12) for c-LaB_6 and (2 2 2) for a-LaB_6. The cut-off energy of 30 Ry (408 eV) was used. All initial structures were optimized by simultaneously relaxing the supercell basis vectors and the atomic positions inside the supercells using the Broyden–Fletcher–Goldfarb–Shanno (BFGS) algorithm [23]. The relaxation of the atomic coordinates and of the supercells was considered to be complete when atomic forces were less than 1.0 mRy/Bohr (25.7 meV/Å), stresses were smaller than 0.05 GPa, and the total energy during the structural optimization iterative process was changing by less than 0.1 mRy (1.36 meV).

The quantum molecular dynamics (QMD) calculations of the initial 56-atoms structure were carried out with fixed unit cell parameters and volume (NVT ensemble, constant number of particles-volume-temperature). The structure was first equilibrated at 5000 K for 3 ps, and then the melts were cooled down to 300 K during 30 ps. The time step was 20 atomic units (about 10^{-15} s). The system temperature was kept constant by rescaling the velocity (tolerance $\sim \pm 50$ K). The variation of the total energy was controlled during each temperature step. The final structure reached its time-averaged equilibrium during the initial calculation time of about 1.8 ps, and afterwards, the total energy of the structures fluctuated only slightly around that equilibrium value. In the case of large-scale QMD simulation, a reduced k-points mesh (2 2 2) was used in order to save computing time without compromising on accuracy. After the QMD equilibration at 300 K, the resultant structure was optimized by simultaneously relaxing the supercell basis vectors and the atomic positions inside the supercells using the BFGS algorithm.

Both the electronic and phonon densities of states (DOS and PHDOS, respectively) were calculated with the tetrahedron method implemented in the "Quantum-ESPRESSO" code. The PHDOSs for both c-LaB_6 and c-LaB_5 were calculated in the framework of the Density-Functional Perturbation Theory (DFPT) [24]. To calculate the phonon density of states of the amorphous LaB_6 phase, the PHONOPY code was used [25].

The elastic moduli of the crystalline and amorphous phases were investigated using the "ElaStic" code [26]. The Vickers hardness was estimated using calculated Young's moduli in the framework of the approach [27].

The tensile stress–strain relations were calculated using by elongating the 56-atom supercells along the c-axis [(001)-direction] in incremental steps, followed by fixing the c basis cell vector and simultaneously relaxing the a- and b-basis cell vectors, and the positions of the atoms within the supercell. The stress of the structures under the shear strain (001)[100] was calculated as follows: first, an incremental shear distortion was imposed, then the basis supercell vectors and the atomic coordinates were relaxed with fixed angles. For both tensile and shear strains the structural parameters at a previous step were used to calculate the Hellmann–Feynman stress for the next step.

3. Results and discussions

In Fig. 1, we show the supercells of c-LaB_6 and a-LaB_6. One can see that the cubic crystalline structure of c-LaB_6 (space group Pm3m, No. 221) consists of the boron octahedron network in which the lanthanum

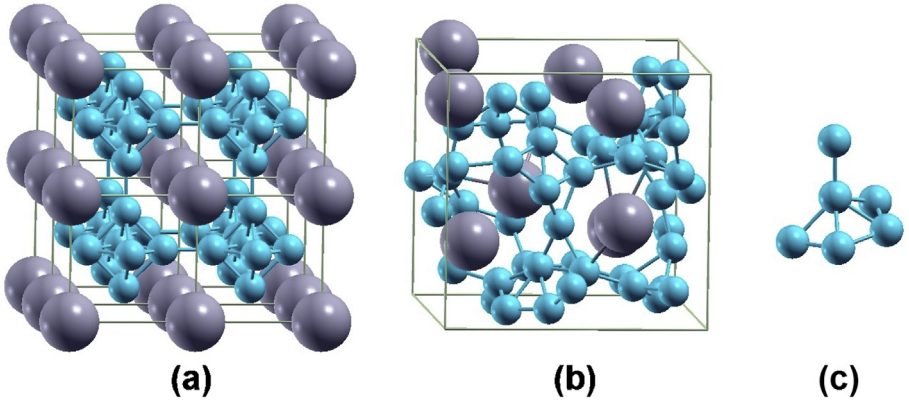

Fig. 1. (2 × 2 × 2) translated cell for c-LaB_6 (a); supercell for a-LaB_6 (b); the fragment of a boron icosahedron in a-LaB_6 (c). Large and small circles are La and B atoms, respectively.

atoms are embedded. The calculated lattice parameter of 4.155 Å is consistent with the experimental value of 4.157 Å [4]. In the case of the amorphous structure, the lanthanum atoms are chaotically distributed, and the B-B network is amorphous and consists of the icosahedron fragments (cf. Fig. 1c). Here it should be noted that the similar boron network was observed for amorphous $AlMgB_{14}$-based materials [28]. The structural functions (PCF, g(Θ)), presented in Fig. 2, confirm the amorphous structure of a-LaB_6: the peaks in the pair correlation functions and bond angle distributions for the amorphous structure are smearing compared to those for the crystalline counterpart. The nearest neighbour B-B correlations in a-LaB_6 are close to those in c-LaB_6.

The densities of states of both the crystalline and amorphous structures are shown in Fig. 3. For c-LaB_6, the detail information about the origin of the main peaks was done in Refs. [8,9,11]. Therefore, for this phase, we note only that the peaks around −17.5 eV and −15.0 eV are originated from La 5p and B 2s+2p states, respectively. The DOS in the ranges from −11.0 eV to −7.0 eV and from −7.0 eV to −2.0 eV is constituted by the B 2s+2p – La 5d and B 2p – La 5d bonding states, respectively. Finally, the DOS above the Fermi level originates mainly from the antibonding B 2p – La 5d states and the La 4f states. Fig. 3a shows that the La 4f states form a sharp peak at 2.0 eV above the Fermi level. Here it should be noted that the distribution of the La states shown in Fig. 3 is consistent with that reported in Refs. [19,20] for other La-based compounds. In Table 1, the local partial Löwdin charges (Q_i) and effective charges (Q_{ef}) for the La and B ions in the crystalline and amorphous LaB_6 are summarized. For the sake of comparison, we present also the charges that where calculated neglecting the La 4f states. Taking into account of the La 4f core-level states in the band structure calculations was found to lead to a reduction of the effective charges. The effective charges decrease on going from c-LaB_6 to a-LaB_6. The latter is supposed to be due to a reduction of the La-B bond lengths because of a randomization of the surrounding of the La atoms after amorphization (cf. Fig. 2). For both the phases, the charge is transferred from the La ions towards the B ions, indicating the availability of the ionic component in chemical bonding.

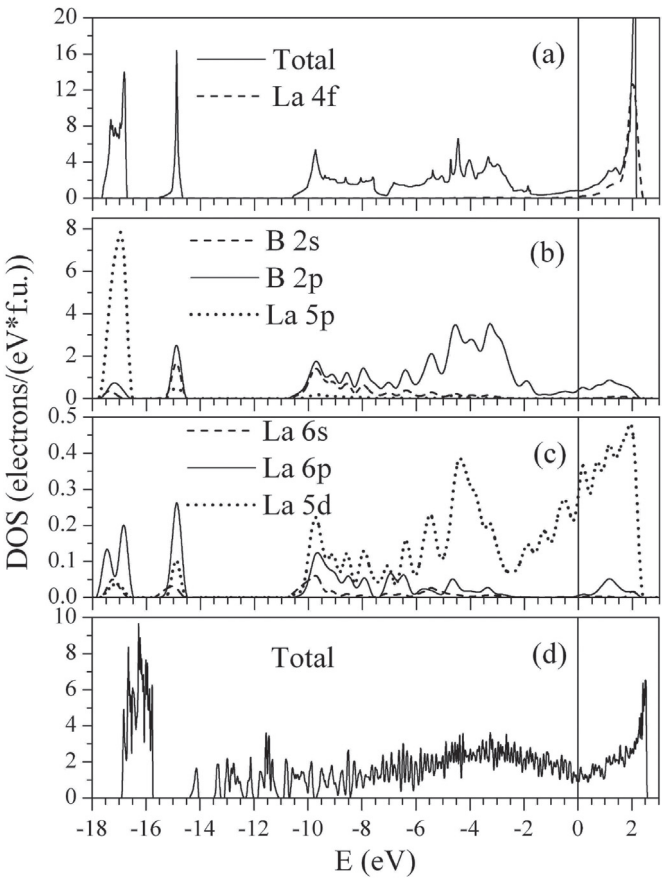

Fig. 3. Total and local partial density of states (DOS) for crystalline (a–c) and amorphous (d) lanthanum hexaborides. The vertical line denotes the Fermi level.

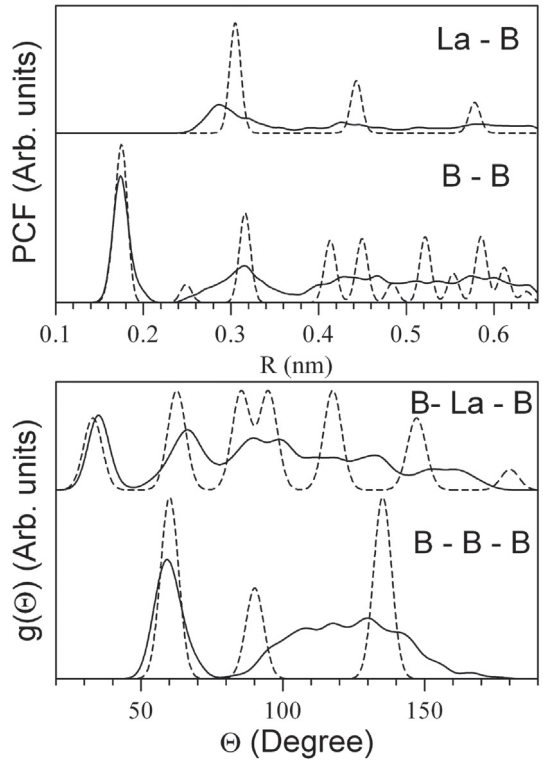

Fig. 2. Pair correlation functions (PCF) and bond angle distribution (g(Θ)) for c-LaB_6 (dashed line) and a-LaB_6 (solid line).

Table 1
Löwdin local partial charges (Q_i) and effective charges (Q_{ef}) for the La and B ions in c-LaB_6 and a-LaB_6 (in *e*). The charges calculated without allowing for the La 4f states are in the parentheses.

Phase	Species	Q_s	Q_p	Q_d	Q_f	Q_{tot}	Q_{ef}
c-LaB_6	La	2.04	6.46	1.63	0.27	10.40	+0.60
		(2.05)	(6.48)	(1.75)	(0.00)	(10.28)	(+0.72)
	B	0.61	2.49	0.00	0.00	3.10	−0.10
		(0.62)	(2.50)	(0.00)	(0.00)	(3.12)	(-0.12)
a-LaB_6	La	2.08	6.45	1.77	0.26	10.56	+0.44
	B	0.63	2.44	0.00	0.00	3.07	−0.07

For the amorphous phase, all the DOS peaks are smearing, and the Fermi level shifts towards the DOS minimum that separates the bonding and antibonding states (cf. Fig. 3b). Taking into account the fact that the states in the DOS minimum of amorphous semiconductors are localized [29], one can suggests that a-LaB_6 will show semiconductor properties. It follows that amorphization of c-LaB_6 will lead to the change of the metallic conductivity to semiconductive one.

The Fermi surface for c-LaB_6 is shown in Fig. 4. The 14th band is located around the Fermi level, and the Fermi surface of this band consists of the semi-spherical electronic shits aligned along the Γ - X direction. The thorough analysis of the Fermi surface enabled us to aim at conclusion that it did not show any nesting regions that could give rise to phonon anomalies.

In Fig. 5 we show the phonon spectra of crystalline and amorphous lanthanum borides. The comparison of the calculated phonon density of states for c-LaB_6 with the experimental spectra is done in Fig. 6. Our PHDOS agrees well with the phonon spectrum calculated in Ref. [10] (not shown here). The characteristic feature of the spectra is the availability of a

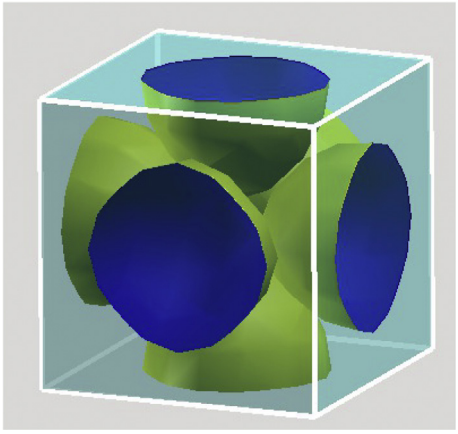

Fig. 4. Fermi surfaces of the 14th band for c-LaB_6.

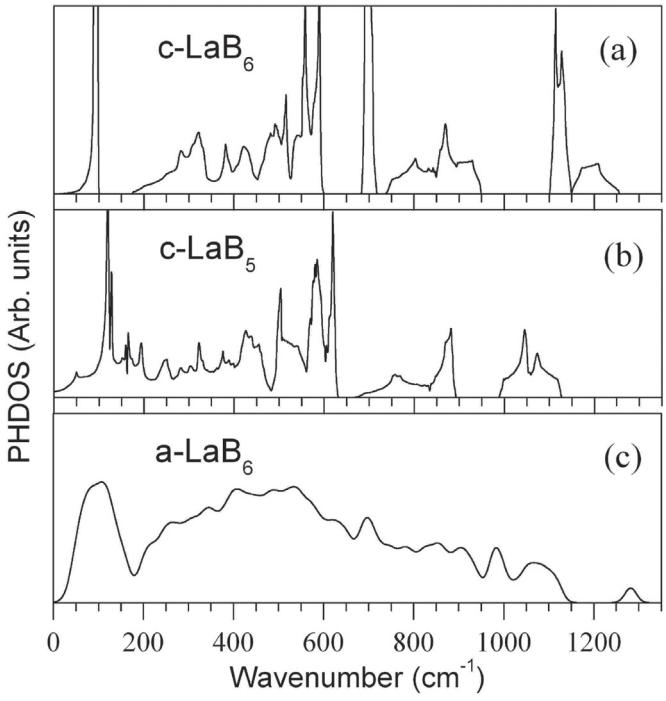

Fig. 5. Phonon densities of states (PHDOS) for: c-LaB_6 determined by using DFPT (a); c-LaB_5 determined by using DFPT (b); a-LaB_6 calculated with the help of the PHONOPY code (c).

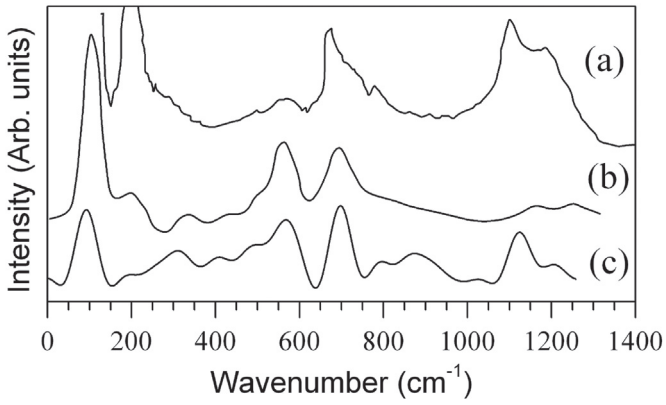

Fig. 6. Experimental and calculated spectra for c-LaB_6: Raman spectrum [30] (a); Point contact spectrum [31] (b); Calculated PHDOS smoothed with a fast Fourier transform (FFT) filter (c).

sharp peak at 100 cm^{-1}. This peak is shown also in the spectrum of sub-stoichiometric LaB_5 (cf. 5b). Given the shape of the Fermi surface, we suppose that this peak is not related to the Fermi surface, and it can be caused by the vibration of the lanthanum atoms that are heavier than the boron atoms. In the case of the amorphous structure, a-LaB_6, the sharp PHDOS peaks are smeared. Nevertheless, the feature at 100 cm^{-1} is shown.

Coming back to Fig. 6, one can see that, for c-LaB_6, the theoretical PHDOS does not reproduce correctly the peak at 200 cm^{-1} in the experimental spectra. However, this peak is observed in the PHDOS of c-LaB_5 (cf. Fig. 5b), for which reason we suggest that the boron vacancies can give rise to the feature around 200 cm^{-1}.

The calculated and experimental heat capacities (C_p) as functions of temperature for both the crystalline and amorphous phases are presented in Figs. 7 and 8. The variation of entropy (S) with temperature is shown

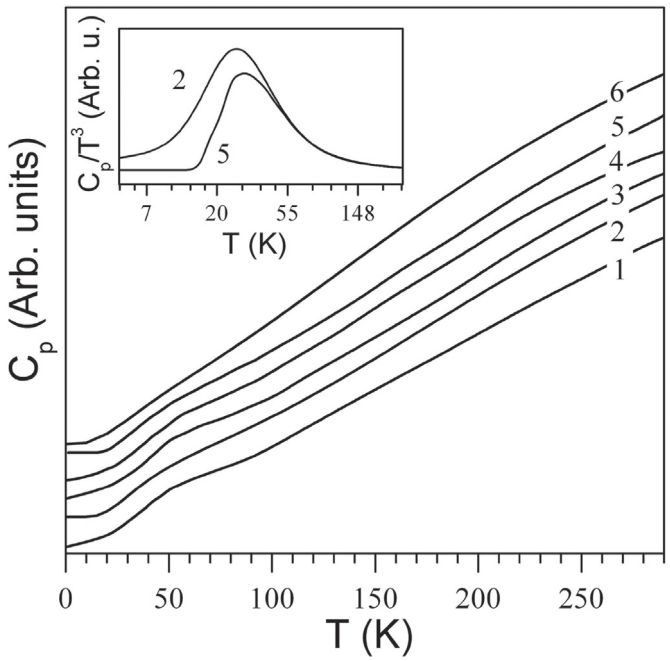

Fig. 7. Specific heat C_p vs. temperature T for c-LaB_6: 1- Ref. [32], 2- the result of our calculations, 3- Ref. [33], 4- Ref. [34], 5- Ref. [2]. In the insert, the C_p/T^3 ration is shown as a function of temperature (T is in the natural logarithmic scale) for the curves 2 and 5. The curve 6 is the C_p(T) dependence for a-LaB_6.

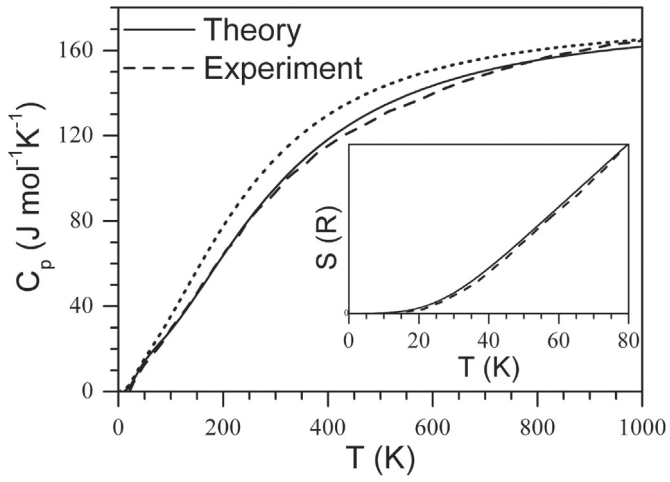

Fig. 8. Calculated (solid line) and experimental [35] (dashed line) specific heat C_p vs. temperature T for c-LaB_6. In the insert, the calculated and experimental [36] entropies for c-LaB_6 (in unit of the gas constant, R) are presented as functions of temperature. The calculated C_p(T) curve for a-LaB_6 is denoted as dotted line.

Table 2
Calculated elastic constants (c_{ij}) for c-LaB_6, Hill bulk modulus (B_H), Hill shear modulus (G_H), Hill Young modulus (E_H), hardness (H), B_H/G_H ratio and Poisson' ratio (ν) for pc-LaB_6 and a-LaB_6. In the parentheses and braces, the experimental and theoretical values of other authors are presented, respectively. For the comparison, the experimental values of Vickers hardness (V_K) and Knoop hardness (H_K) were included. All the values of the moduli are in GPa.

Phase	c_{11}	c_{12}	c_{44}	B_H	G_H	E_H	B_H/G_H	ν	H
c-LaB_6	472	26	87	174	129	310	1.35	0.20	18.8
pc-LaB_6	(453)[a]	(18.2)[a]	(90)[a]	(174)[f]	{133}[e]	(185)[g]	{1.31}[e]	{0.20}[h]	(15)[b]
	{466}[d]	{37}[d]	{88}[d]	{174}[e]	{131}[h]	{319}[e]	{1.33}[h]		(19)[c]
	{473}[e]	{24}[e]	{92}[e]	{174}[h]	{128}[i]	{315}[h]	{1.35}[i]		
	{474}[h]	{24}[h]	{90}[h]	{173}[i]		{450}[i]			
	{454}[i]	{32}[i]	{91}[i]						
a-LaB_6				129	76	191	1.70	0.25	11.2

[a] Ref. [37].
[b] Ref. [38], H_V.
[c] Ref. [39], H_K.
[d] Ref. [40].
[e] Ref. [41].
[f] Ref. [42].
[g] Ref. [43].
[h] Ref. [12].
[i] Ref. [15].

in Fig. 8. For c-LaB_6, the experimental dependence of the heat capacity has an abnormal behavior at 50 K [2,32–34]. The calculated $C_p(T)$ dependence shows the same behavior. We calculated the $C_p(T)$ function with and without the peak at 100^{-1} cm in the PHDOS (not shown here) and arrived at a conclusion that the mentioned peculiarity at 50 K is caused by the peak at 100 cm^{-1} in the phonon density of states. Both the calculated $C_p(T)$ and S(T) dependences are in agreement with the corresponding experimental functions.

Coming back to the amorphous lanthanum hexaboride, we see that the peculiarity at 50 K in the $C_p(T)$ dependence disappears. This is caused by the smearing of the peak at 100 cm^{-1} in the PHDOS of a-LaB_6 (cf. Fig. 5). Fig. 8 shows that, in the temperature range of 0–1000 K, the heat capacity of a-LaB_6 is higher compared to that of c-LaB_6. It follows that the thermal conductivity of lanthanum hexaboride will decrease after the amorphization of the crystalline material. This finding is confirmed by the results of the calculations of the Debye temperature (see below).

The elastic constants for c-LaB_6, pc-LaB_6 and a-LaB_6 were calculated using the "ElaStic" code [26]. The calculated elastic constants for c-LaB_6, as well the bulk, shear, Young moduli, Poisson's ratio and hardness for polycrystalline and amorphous LaB_6 are presented in Table 2. For c- and pc-LaB_6, the calculated values are in the good agreement with the corresponding experimental and theoretical characteristics. The elastic moduli and hardness of amorphous LaB_6 are lower compared to those of pc-LaB_6 approximately by 30–40%. An analysis of the atomic configuration of the crystalline and amorphous phases of LaB_6 (cf. Fig. 1) shows that the boron octahedrons fail, and the boron icosahedron-like fragments form during amorphization. However, the formation of the distorted icosahedron-like boron network does not lead to strengthening lanthanum hexaboride.

The hardness of the materials was determined at equilibrium, however, their hardness were measured during deformation, i.e., in a non-equilibrium state. We calculated the stress-strain curves for both c-LaB_6 and a-LaB_6. The calculated curves are shown in Fig. 9. The ideal tensile and shear strengths (the maximum stress before failure) were 42.1 GPa and 28.1 GPa, respectively, for c-LaB_6, as well as 13.2 GPa and 13.7 GPa, respectively, for a-LaB_6. These values are higher compared to the calculated hardnesses (cf. Table 2). It follows that our estimation of the hardness is quite plausible. For c-LaB_6, we determined the Young's modulus from the tensile stress-strain curve at the strain equal to 0.04 (cf. Fig. 9). The estimated Young's modulus is 431 GPa that is very close to the experimental value of 428 GPa for LaB_6 single crystal [43]. The microhardness of the (001) plane of LaB_6 single crystal under a load of 0.98 N was found to be 25 GPa [44]. This value is comparable with the ideal shear strength of 28.1 GPa for c-LaB_6 (cf. Fig. 9). The latter comparison is based on the fact that the ideal shear strength of a material correlates with its hardness [45].

The B/G ratio provides the information about the ductility of a material: it will be ductile, if the B/G ration will be higher than 1.75, otherwise it will be brittle. The values of Poisson's ratios ν correlate with B/G. A material will be ductile provided $\nu > 0.26$ [37]. The values of the

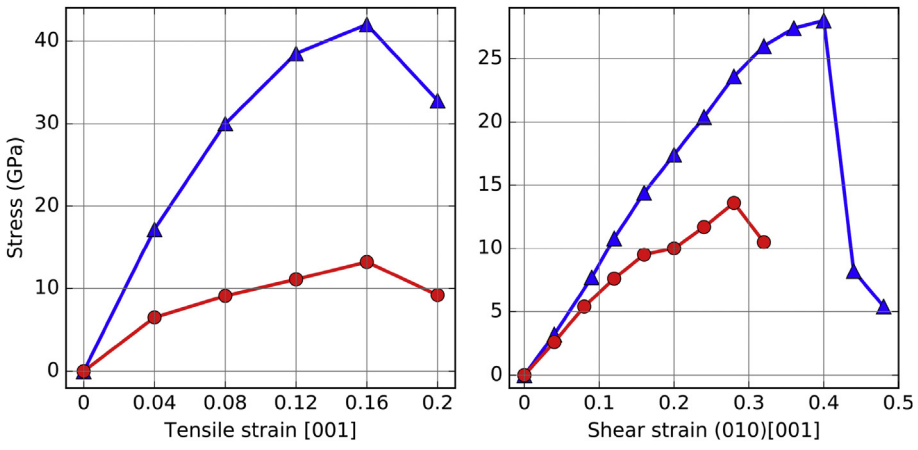

Fig. 9. Stress-strain relations for c-$LaBa_6$ (triangles) and a-$LaBa_6$ (circles).

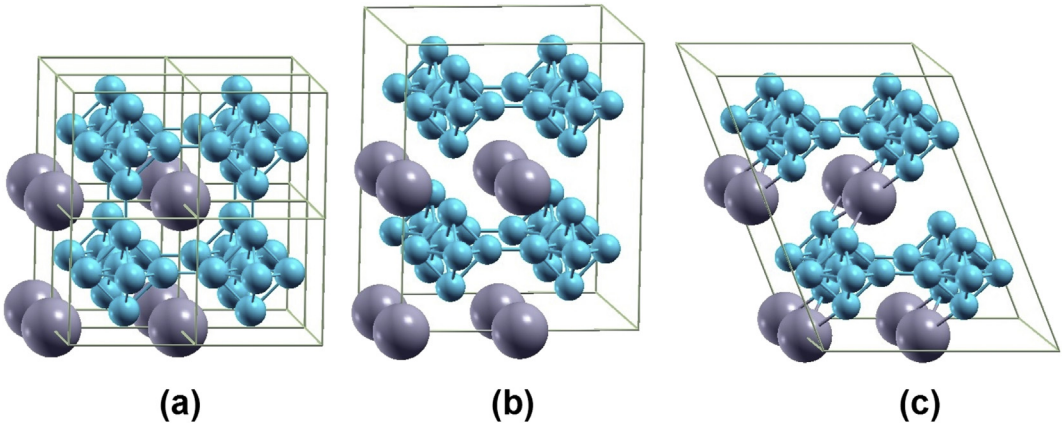

Fig. 10. Atomic configurations of c-LaB_6 in the equilibrium (a), and after failure under tensile strain (b) and shear strain (c). The large and small circles are lanthanum and boron atoms, respectively.

B_H/G_H ratio and Poisson's ratio for pc- LaB_6 and a-LaB_6 are also sown in Table 2. The values of B_H/G_H of both the pc- and a-phases of LaB_6 are lower than 1.75 and 0.26, respectively, indicating that these materials should be brittle. However, since for a-LaB_6 the values of B_H/G_H (1.70) and ν (0.25) approach 1.75 and 0.26, respectively, one can expect that it will exhibit the mechanical properties that will be close to those of a ductile material.

The mechanism of the failure of c-LaB_6 under tensile and shear strains can be understood from Fig. 10, where the atomic configurations of c-LaB_6 at different stages of strains are shown. It is clearly seen that the failure of the structure occurs due to breaking inter-octahedron B-B bonds, and the boron octahedrons remains undistorted at that.

It is well known that, in thermodynamics and mechanics, an important fundamental parameter of materials is Debye temperature Θ_D. Since we have calculated already the elastic moduli, it is appropriate to use these values to estimate the Debye temperature. Therefore we used the standard method that is based on the knowledge of elastic constant data, transverse and longitudinal sound velocities [46]:

$$\Theta_D = \frac{h}{k_B}\left(\frac{3n}{4\pi}\left[\frac{N_A\rho}{M}\right]\right)^{1/3}\left(\frac{1}{3}\left[\frac{2}{v_t^3}+\frac{1}{v_l^3}\right]\right)^{-1/3},$$

$$v_t = (G_H/\rho)^{1/2}, \quad v_l = ([B_H + 4G_H/3\rho])^{1/2},$$

where h/k_B have the usual meanings of quantum mechanics, n is the number of atoms in the molecule, N_A is Avogadro's number, ρ is the density, M is the molecular weight, v_t is the transverse sound velocity and v_l is the longitudinal sound velocity, B_H and G_H are the Hill bulk modulus and Hill shear modulus, respectively (cf. Table 2).

In Table 3, we present the calculated density (ρ), transverse (v_t), longitudinal (v_l) and average (v_m) sound velocities and Debye temperatures (Θ_D) for the crystalline and amorphous phases of LaB_6. The experimental results on Θ_D for c-LaB_6 are also shown. The experimental values of Θ_D are strongly scattered. One can see that the calculated Debye temperature for c-LaB_6 agrees well with Θ_D reported in Refs. [32] and [48] (within 2.5%). Unfortunately, we did not find any experimental and theoretical results on the Debye temperature of a-LaB_6. We would like to remind that a higher Debye temperature is associated with a larger thermal conductivity. Owing to the low density and structural disorder, the value of Θ_D for a-LaB_6 is lower compared to the Debye temperature for c-LaB_6. This means that the thermal conductivity of the amorphous phase will be worse than the crystalline material.

Table 3
Density (ρ), transverse (v_t), longitudinal (v_l) and average (v_m) sound velocities and Debye temperatures (Θ_D) for the crystalline and amorphous phases of LaB_6.

Phase	ρ (g/cm^3)	v_t (m/s)	v_l (m/s)	v_m (m/s)	Θ_D (K)
c-LaB_6	4.72	5230.3	8565.8	5775.4	791 (212–885)[a] (773)[b] (773)[c]
a-LaB_6	4.52	4098,4	7134.9	4551.7	615

[a] Ref. [47].
[b] Ref. [32].
[c] Ref. [48].

4. Conclusions

We calculated the electronic properties, phonon structure, thermodynamic properties, elastic constants and mechanical properties of crystalline and amorphous lanthanum borides using a first principles pseudopotential method and molecular dynamics realized in the "Quantum ESPRESSO" code. The amorphous material represents the random distributed La atoms embedded into the amorphous icosahedron-like boron matrix. In contrast to c-LaB_6, the amorphous phase is suggested to show semiconductor properties. For c-LaB_6, an analysis of the calculated phonon spectra and the Fermi surface indicates that the sharp peak at 100 cm^{-1} in the phonon density of states is not related to the shape of the Fermi surface. It was shown that the feature at 50 K in the $C_p(T)$ dependence is caused by the availability of this peak in the phonon spectrum. The calculated elastic moduli and hardness for the polycrystalline LaB_6 structure are higher approximately by 30–40% compared to those of the amorphous counterpart. This tendency is observed also for the ideal tensile and shear strengths, which is due to the failure of boron octahedrons in the amorphous phase. The failure of c-LaB_6 occurs mainly because of the breaking of the inter-octahedron boron bonds, and the boron octahedrons remain undistorted at that. For crystalline and polycrystalline LaB_6, the calculated elastic moduli, hardness, Debye temperature, phonon density of states as well as the dependences of heat capacity and entropy on temperature are in good agreement with the corresponding experimental characteristics. We hope that the results of our calculations will useful for the technologists working in the field of the synthesis of LaB_6 for its application as an electron emitter and a hard material for wear-resistant coatings.

Acknowledgments

This work was supported by the contract of NAS of Ukraine No. III-9-15. The work of P. T. was performed under the auspices of the U. S. Department of Energy by the Lawrence Livermore National Laboratory under contract No. DE-AC52-07NA27344. The authors are grateful to the directorate of the Summer Institute at Jackson State University for the opportunity to perform large-scale calculations.

References

[1] M. Aono, R. Nishitani, C. Oshima, T. Tanaka, E. Bannai, S. Kawai, Direct observation of LaB_6(001) surface at high temperatures by x-ray and ultraviolet photoelectron spectroscopy, low energy electron diffraction, auger electron spectroscopy, and workfunction measurements, J. Appl. Phys. 50 (7) (1979) 4802–4807.

[2] D. Mandrus, B.C. Sales, R. Jin, Localized vibrational mode analysis of the resistivity and specific heat of LaB_6, Phys. Rev. B 64 (1) (2001), 012302.

[3] K.C. Qi, Z.L. Lin, W.B. Chen, G.C. Cao, J.B. Cheng, X.W. Sun, Formation of extremely high current density LaB_6 field emission arrays via e-beam deposition, Appl. Phys. Lett. 93 (9) (2008), 093503–3.

[4] S. Otani, S. Honma, Y. Yajima, Y. Ishizawa, Preparation of LaB_6 single crystals from a boron-rich molten zone by the floating zone method, J. Cryst. Growth 126 (2–3) (1993) 466–470.

[5] Y. Kato, Y. Ono, Y. Akita, M. Hosaka, N. Shiraishi, N. Tsuchimine, S. Kobayashi, M. Yoshimoto, Fabrication and characterization of electrically functional lanthanum hexaboride thin films on ultrasmooth sapphire substrates, Mater. Res. Soc. Symp. Proc. 1148 (2009). PP12–02.

[6] E. Nebauer, XRD investigations of WSiN and LaB_6 layers on GaAs, Phys. Status Solid. B 194 (1) (1996) 121–126.

[7] J.H. Choi, H.Y. Ahn, Y.S. Lee, M.H. Yang, C.-W. Baik, K.S. Cho, S.I. Kim, S.-J. Jeong, J.-M. Jeon, M. Kim, S. Hwang, Local crystallization of LaB_6 yielding compact, strong thermionic electron emission source, IEEE Electron. Dev. Lett. 34 (10) (2013) 1322–1324.

[8] F.M. Hossain, D.P. Riley, G.E. Murch, Ab initio calculations of the electronic structure and bonding characteristics of LaB_6, Phys. Rev. B 72 (2005) 235101–235105.

[9] S. YuChang, X. LiHua, F. YunChang, Z. PengFei, P. Ping, First-principles calculation on the electronic structure and optical properties of LaB_6, Sci. Sin. Phys. Mech. Astron. 41 (1) (2011) 58–65.

[10] L. Chao, L. Bao, W. Wei, O. Tegus, Optical properties of Yb-doped LaB6 from first-principles calculation, Mod. Phys. Lett. B 30 (7) (2016) 1650091–1650097.

[11] L. Chao, L. Bao, W. Wei, T. O, Z. Zhang, First-principles study on the electronic structure, phonons and optical properties of LaB_6 under high-pressure, J. Alloy. Comp. 672 (2016) 419–425.

[12] X. Zeng, Y. Ye, S. Zou, Q. Gou, Y. Wen, P. Ou, First-principles study of the nonlinear elasticity of rare-earth hexaborides REB6 (RE = La, Ce), Crystals 7 (2017) 320.

[13] C.H. Chen, T. Aizawa, N. Iyi, A. Sato, S. Otani, Structural refinement and thermal expansion of hexaborides, J. Alloy. Comp. 366 (2004) L6–L8.

[14] A. Baranovskiy, G. Grechnev, V. Fil, T. Ignatova, A. Logosha, A. Panfilov, I. Svechkarev, N. Shitsevalova, V. Filippov, O. Eriksson, Electronic structure, bulk and magnetic properties of MB_6 and MB_{12} borides, J. Alloy. Comp. 442 (2007) 228–230.

[15] Kan Luo, Yingjie Qiao, Shihong He, Xian-Hu Zha, Qing Huang, Jian He, Cheng-Te Lin, Joseph S. Francisco, Shiyu Du, Crystal structures and mechanical properties of M(Mg, Sr, Ba, La)xCa1−xB6 solid solution: a first principles study 42 (6) (2016) 6632–6639.

[16] B. Huang, Y.-H. Duan, Y. Sun, M.-J. Peng, S. Chen, Electronic structures, mechanical and thermodynamic properties of cubic alkaline-earth hexaborides from first principles calculations, J. Alloy. Comp. 635 (2015) 213–224.

[17] H. Kasai, E. Nishibori, Spatial distribution of electrons near the Fermi level in the metallic LaB6 through accurate X-ray charge density study, Sci. Rep. 7 (2017) 41375–41379.

[18] P. Giannozzi, S. Baroni, N. Bonini, M. Calandra, R. Car, C. Cavazzoni, D. Ceresoli, G.L. Chiarotti, M. Cococcioni, I. Dabo, A. Dal Corso, S. de Gironcoli, S. Fabris, G. Fratesi, R. Gebauer, U. Gerstmann, C. Gougoussis, A. Kokalj, M. Lazzeri, L. Martin-Samos, N. Marzari, F. Mauri, R. Mazzarello, S. Paolini, A. Pasquarello, L. Paulatto, C. Sbraccia, S. Scandolo, G. Sclauzero, A.P. Seitsonen, A. Smogunov, P. Umari, R.M. Wentzcovitch, QUANTUM ESPRESSO: a modular and open-source software project for quantum simulations of materials, J. Phys. Condens. Matter 21 (39) (2009) 395502–395519.

[19] S.D. Gupta, S.K. Gupta, P.K. Jha, First-principles lattice dynamical study of lanthanum nitride under pseudopotential approximation, Comput. Mater. Sci. 49 (2010) 910–915.

[20] X.Z. Yan, Y.M. Chen, X.Y. Kuang, S.K. Xiang, Theoretical investigation of La monopnictides: electronic properties and pressure-induced phase transition , J. Appl. Phys. 116 (2014) 083707.

[21] J.P. Perdew, K. Burke, M. Ernzerhof, Generalized gradient approximation made simple, Phys. Rev. Lett. 77 (18) (1996) 3865–3868.

[22] D. Vanderbilt, Soft self-consistent pseudopotentials in a generalized eigenvalue formalism, Phys. Rev. B 41 (11) (1990) 7892–7895.

[23] S.R. Billeter, A. Curioni, W. Andreoni, Efficient linear scaling geometry optimization and transition-state search for direct wavefunction optimization schemes in density functional theory using a plane-wave basis, Comput. Mater. Sci. 27 (4) (2003) 437–445.

[24] S. Baroni, S. de Gironcoli, A. Dal Coro, P. Giannozzi, Phonons and related crystal properties from density-functional perturbation theory, Rev. Mod. Phys. 73 (2) (2001) 515–562.

[25] A. Togo, Phonopy, https://atztogo.github.io/phonopy/.

[26] R. Golesorkhtabar, P. Pavone, J. Spitaler, P. Puschnig, C. Draxl, Elastic: a tool for calculating second order elastic constants from first principles, Comput. Phys. Commun. 184 (8) (2011) 1861–1873.

[27] X. Jiang, J. Zhao, X. Jiang, Correlation between hardness and elastic moduli of the covalent crystals, Comput. Mater. Sci. 50 (7) (2011) 2287–2290.

[28] V.I. Ivashchenko, P.E.A. Turchi, S. Veprek, V.I. Shevchenko, J. Leszczynski, L. Gorb, F. Hill, First-principles study of crystalline and amorphous $AlMgB_{14}$-based materials, J. Appl. Phys. 119 (20) (2016) 205105.

[29] V.I. Ivashchenko, P.E.A. Turchi, V.I. Shevchenko, L.A. Ivashchenko, O.A. Shramko, Simulations of pressure-induced phase transitions in amorphous Si_xC_{1-x} alloys, Phys. Rev. B 71 (16) (2005), 165209–9.

[30] R. Schmechel, H. Werheit, Yu.B. Paderno, FT Raman spectroscopy of some metal hexaborides, J. Solid State Chem. 133 (1) (1997) 264–268.

[31] P. Samuely, M. Reiffers, K. Flachbart, A.I. Akimenko, I.K. Yanson, N.M. Ponomarenko, Yu.B. Paderno, Point-contact spectroscopy of the electron-phonon interaction in single-crystal LaB_6, J. Low Temp. Phys. 71 (1–2) (1988) 49–61.

[32] H.G. Smith, G. Dolling, S. Kunii, M. Kasaya, B. Liu, K. Takegahara, T. Kasuya, T. Goto, Experimental study of lattice dynamics in LaB_6 and YbB_6, Solid State Commun. 53 (1) (1985) 15–19.

[33] Yu.B. Paderno, N. Shizevalova, V. Muratov, Boridy, Institute for Problems of Materials Science, Akad. Nauk Ukrainian SSR, 1991 (in Russian).

[34] Y. Peysson, C. Ayache, B. Salce, J. Rossat-Mignod, S. Kunii, T. Kasuya, Thermal properties of CeB_6 and LaB_6, J. Magn. Magn Mater. 47–48 (1985) 63–65.

[35] Report of National Institute for Researches in Inorganic Materials, No 17, Tsukuba, Japan, 1978, p. 44 (in Japanese).

[36] T. Fujita, M. Suzuki, Y. Ishikawa, Specific heat of EuB_6, Solid State Commun. 33 (9) (1980) 947–950.

[37] T. Tanaka, J. Yoshimoto, M. Ishii, E. Bannai, S. Kawai, Elastic constants of LaB_6 at room temperature, Solid State Commun. 22 (3) (1977) 203–205.

[38] S. Otani, T. Tanaka, Y. Ishizawa, Crystal quality and high temperature hardness of LaB_6 crystals prepared by the floating zone method, J. Alloy. Comp. 202 (1–2) (1993) L25–L28.

[39] V.N. Gurin, L.I. Derkachenko, M.M. Korsukova, S.P. Nikanorov, W. Jung, R. Müller, Sov. Phys. Solid State 38 (1996) 1508.

[40] T. Gürel, R. Eryiğit, *Ab initio* lattice dynamics and thermodynamics of rare-earth hexaborides LaB_6 and CeB_6, Phys. Rev. B 82 (2010), 104302.

[41] D. Jie, Z. Tong, Z. Li, D. Ji-Guang, J. Gang, W. Hong-Bin, Elastic properties and electronic structures of lanthanide hexaborides, Chin. Phys. B 24 (9) (2015) 096201–096209.

[42] B.K. Godwal, E.A. Petruska, S. Speziale, J. Yan, S.M. Clark, M.B. Kruger, R. Jeanloz, High-pressure Raman and x-ray diffraction studies on LaB_6, Phys. Rev. B 80 (17) (2009), 172104.

[43] H. Zhang, J. Tang, L. Zhang, B. An, L.-C. Qin, Atomic force microscopy measurement of the Youngs modulus and hardness of single LaB_6 nanowires, Appl. Phys. Lett. 92 (17) (2008) 173121–173123.

[44] S.N. Dub, G.P. Kislaya, P.I. Loboda, Study of mechanical properties of LaB_6 single crystal by nanoindentation, J. Superhard Mater. 35 (3) (2013) 158–165.

[45] V.I. Ivashchenko, S. Veprek, A. Argon, P.E.A. Turchi, L. Gorb, F. Hill, J. Leszczynski, First-principles quantum molecular calculations of structural and mechanical properties of TiN/SiN_x heterostructures, and the achievable hardness of the nc–TiN/SiN_x nanocomposites, Thin Solid Films 578 (2015) 83–92.

[46] S. Chen, Y. Sun, Y.-H. Duan, B. Huang, M.-J. Peng, Phase stability, structural and elastic properties of C15-type Laves transition-metal compounds MCo2 from first-principles calculations, J. Alloy. Comp. 630 (2015) 202–208.

[47] M.M. Korsukova, T. LundstrSm, L.-E. Tergenius, The X-ray Debye temperature of LaB_6, Solid State Commun. 63 (3) (1987) 187–189.

[48] T. Tanaka, T. Akahane, E. Bannai, S. Kawai, N. Tsuda, Y. Ishizawa, Role of polar optical phonon scattering in electrical resistivities of LaB6 and ReO3 (metallic conduction), J. Phys. C Solid State Phys. 9 (1976) 1235–1243.